Chemical Engineering Journal 481 (2024) 148541

Contents lists available at ScienceDirect

Chemical Engineering Journal

journal homepage: www.elsevier.com/locate/cej

One-pot in situ synthesis of expandable graphite-encapsulated paraffin composites for thermal energy storage

Wei Li [a], Chongjie Gao [a], Aolin Hou [b], Jingjing Qiu [d], Shiren Wang [a,b,c,*]

[a] Department of Industrial and Systems Engineering, Texas A&M University, College Station, TX 77843, United States
[b] Department of Materials Science and Engineering, Texas A&M University, College Station, TX 77843, United States
[c] Department of Biomedical Engineering, Texas A&M University, College Station, TX 77843, United States
[d] Department of Mechanical Engineering, Texas A&M University, College Station, TX 77843, United States

ARTICLE INFO

Keywords:
Expandable graphite
Encapsulation
Thermal energy storage
Thermoelectric
Composites

ABSTRACT

To mitigate the intermittency of renewable energy generation and achieve net-zero greenhouse gas emissions, a cyclically stable and energy-efficient thermal energy storage system (TESS) is increasingly required. To prevent leakage and enhance thermal conductivity and stability, TESS is typically fabricated by impregnating energy storage materials (ESMs) into porous conductive additives. However, the impregnation-based encapsulation process is both time-consuming (several to tens of hours) and energy-intensive, and the incorporation of additives reduces the proportion of ESMs, resulting in decreased energy capacity. In this study, we present an ultrafast (several minutes) and energy-efficient one-pot encapsulation method for in situ encapsulation of paraffin wax (PW) within the pores of expanded graphite (EG) via microwave irradiation of expandable graphite (Eg) in molten PW. The resulting binary PW/EG composites exhibit shape stability and no leakage even at 92 wt% PW loading. The PW/EG composite with 10 wt% EG demonstrates a thermal conductivity of 3.7 W/mK (16.2 times higher than that of pure PW), a thermal release/absorption efficiency of around 99.5 %, and almost 100 % capacity retention after thermal cycling. Additionally, we demonstrate that integrating PW/EG TESS with thermoelectric (TE) modules can increase TE power generation by more than fivefold, highlighting their potential for energy storage and conversion as well as mitigating waste heat source intermittency.

1. Introduction

To achieve net-zero greenhouse gas emissions, it is imperative to increase the utilization of renewable energy generation from sources such as photovoltaics, wind, geothermal, and industrial waste heat [1,2]. However, renewable energy is often intermittent and presents challenges in providing stable power when needed [3,4]. Cost-effective and cyclic-stable energy storage systems are crucial for mitigating intermittency and ensuring grid reliability. Thermal energy storage systems (TESS) can reduce peak load and address renewable energy intermittency by time-shifting the load, which is critical for decarbonization and reducing greenhouse gas emissions [5]. Phase change materials (PCMs), including paraffin wax [6–15], fatty acids [16–19], and salt hydrates [20–25], are commonly utilized in TESS due to their high energy density and stability when compared to sensible heat storage materials and thermochemical heat storage systems [26–28].

The limitations of PCMs for TESS include poor heat transfer performance, leakage, and unstable performance during melting/solidification cycles [29]. To address these issues, various strategies have been developed to encapsulate PCMs using thermal conductive materials to improve thermal conductivity and prevent leakage [7,30]. One approach involves incorporating PCMs with polymeric shells using methods such as emulsification [11], in-solution polymerization [24], and stabilizing polymer coating [23]. However, this approach requires non-PCM polymers, long processing times, large amounts of process solvents, and intensive energy to remove the solvents [6,18]. Additionally, this approach necessitates the addition of thermally conductive fillers such as carbon powder and metal particles to enhance thermal conductivity [31,32], further reducing the loading ratio of PCMs. Another approach involves preparing porous matrix materials first, such as expanded graphite (EG), carbon nanotubes, graphene foam, metal foams, porous silica, and zeolite, and then impregnating PCMs into the pores [33–35]. However, the impregnation process is time-consuming and energy-intensive [14,16,17,19], requires the PCMs to remain in a

* Corresponding author at: Department of Industrial and Systems Engineering, Texas A&M University, College Station, TX 77843, United States.
E-mail address: s.wang@tamu.edu (S. Wang).

https://doi.org/10.1016/j.cej.2024.148541
Received 5 August 2023; Received in revised form 26 November 2023; Accepted 2 January 2024
Available online 4 January 2024

molten state throughout the process, and necessitates auxiliary equipment such as vacuum infiltration, ultrasonic vibration, and filtration (Fig. 1a and Table S1). Furthermore, up to 20 wt% of EG or a third encapsulation additive such as a cross-linked polymer network or polymer shell is required to achieve necessary leak resistance and good thermal conductivity, reducing the PCM content in TESS composites (Fig. 1b). Thus, there is a need for a less time-consuming and energy-efficient method to fabricate leak-free and shape-stable PCM composites with both high PCM loading and excellent thermal conductivity.

EG is one of the most used thermally conductive fillers in TESS because of its high thermal conductivity, porous structure, low cost, and chemical stability. EG is usually prepared from expandable graphite (Eg), a graphite intercalation compound, by furnace annealing (up to 900 °C). Upon exposure to a rapid increase in temperature, these intercalation compounds in EG decompose into gaseous products, resulting in highly porous EG with an expansion ratio of up to 300 times [36]. In addition to thermal expansion, EG can also be produced by microwave irradiation, where the conductive graphene layers of Eg convert microwave energy into heat and locally raise the temperature of the intercalation compound to gasify [37,38]. Locally expanding Eg in molten PCM via microwave irradiation and simultaneously encapsulating PCM in situ within the voids of newly formed EG appears to be a promising approach for fabricating PCM/EG composites. Microwave irradiation is becoming increasingly popular in PCM composite fabrication due to its time and energy efficiency. For instance, Zhang et al. discovered that EG, when prepared at an irradiation power of 800 W for 10 s, demonstrated a maximum sorption capacity of 92 wt% for paraffin [37]. Li et al. used microwave radiation in a hydrogen peroxide solution to treat flake graphite (FG), which was then used to support stearic acid (SA) in the synthesis of SA/FG composites for thermal energy storage [39]. Rivero et al. reported on the microwave-assisted modification of starch for compatibilizing LDPE/starch blends [40]. Sundararajan et al. prepared a shape-stabilized PCM composite using microwave-assisted blending of PEG and cellulose acetate (CA) [41]. However, most current applications of microwave irradiation in PCM composites focus on the fabrication of additives like EG or the blending of polymeric materials, based on the absorption of microwaves by dipole active molecules. Despite the use of microwave irradiation, these methods still necessitate a time and energy-consuming impregnation process. To the best of our knowledge, the in-situ encapsulation of PCMs within thermally conductive materials such as Eg has not been explored yet. Compared with conventional multi-step encapsulation methods, this one-pot approach has the potential to significantly reduce fabrication time from hours to minutes and eliminate the need for process solvents and complex impregnation-support equipment (Fig. 1).

In this study, we present a one-pot method for expanding expandable graphite in molten PCMs via microwave irradiation while simultaneously encapsulating PCMs in situ within the voids created by expansion. Paraffin wax (PW) is used as the PCM due to its low melting point (53–58 °C) and high boiling point (370 °C), low supercooling, excellent chemical stability, high latent heat, and non-toxicity [30,42,43]. The resulting binary PW/EG composite exhibits no leakage even with a PW content as high as 92 wt%. The PW/EG composite with 10 wt% EG demonstrates a thermal conductivity of 3.7 W/mK, a thermal release/absorption efficiency above 99.5 %, and a capacity retention rate of 99.6 % after 100 thermal cycles. Furthermore, we have demonstrated the use of PW/EG composites in combination with thermoelectric modules for simultaneous thermal energy storage and conversion.

2. Experimental section

2.1. Materials

Paraffin wax and expandable graphite (50 mesh, around 300 μm) were obtained from Sigma-Aldrich. Paraffin wax (PW) has a melting point of 53–58 °C and a boiling point greater than 370 °C. Expandable graphite (Eg) is a synthesized intercalation compound of graphite that expands or exfoliates when heated. This material is produced by treating flake graphite with various intercalation reagents (<5 wt%) that migrate between the graphene layers in a graphite crystal and remain as stable species (Fig. 2a). Upon exposure to a rapid increase in temperature via microwave irradiation (Supplementary video 1), these intercalation compounds decompose into gaseous products (nitrogen oxides and sulfur oxides), resulting in high inter-graphene layer pressure [36]. This pressure generates sufficient force to push apart graphite basal planes in the "c" axis direction, leading to an increase in the volume of the graphite of up to 300 times (Fig. 2b, and Figs. S1 and S2).

2.2. One-pot preparation of PW/EG composite via microwave irradiation

The fabrication process of the PW/EG composite via in situ encapsulation is depicted in Fig. 2c. PW was melted in a glass beaker by heating it to 80 °C on a hot plate. Eg (2–20 wt%) was added to the molten PW and allowed to settle naturally at the bottom of the beaker. The beaker was covered with a glass petri dish, with the spout serving as a channel for gas flow. The beaker was then placed in a microwave oven (Samsung, 1100 W) and irradiated for 30 s. During irradiation, the Eg absorbed microwave energy and generated localized heat, partially expanded, and produced gases that expelled air through the beaker spout, preventing PW ignition. Simultaneously, PW diffused into the

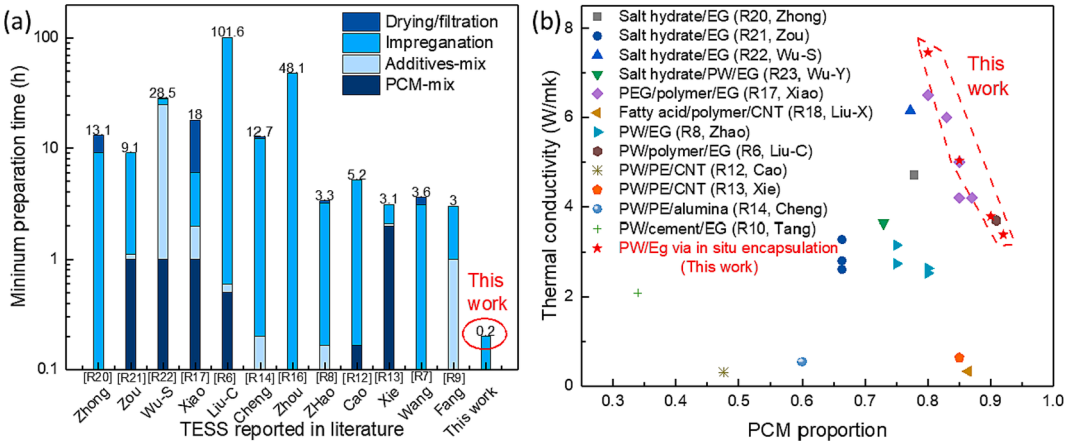

Fig. 1. Comparison of fabrication processes and energy storage performance of thermal energy storage systems (TESS) reported in the literature and in this work. (a) Comparison of fabrication steps and minimum fabrication times for various TESS materials [6–9,12–14,16,17,20–22]. (b) Comparison of thermal conductivity and PCM proportion for various TESS materials [6,8,10,12–14,17,18,20–23]. Detailed information is provided in Table S1.

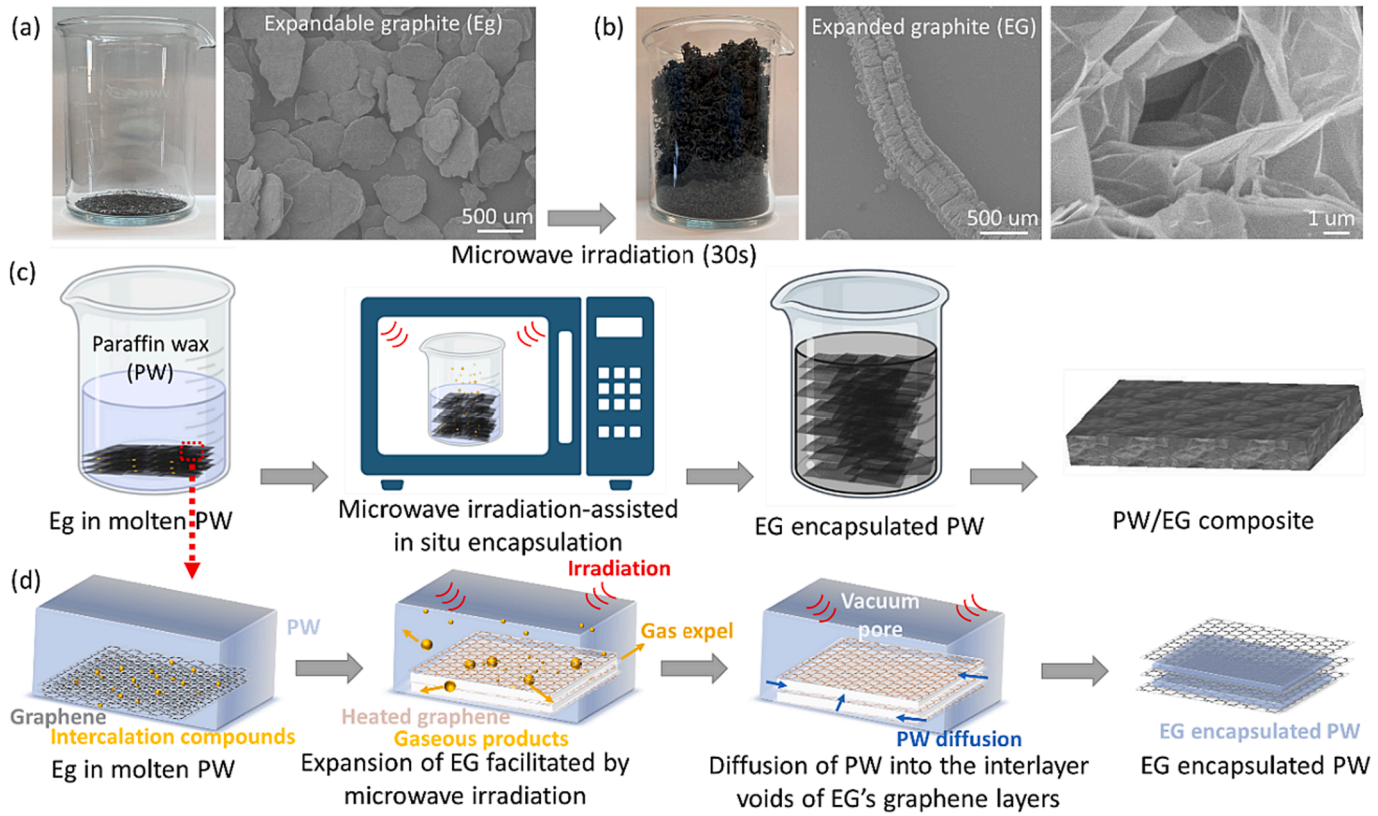

Fig. 2. In-situ encapsulation of PW in EG through microwave irradiation. (a) Optical and SEM images of Eg. (b) Morphologies of EG produced by microwave irradiation of Eg. (c) Schematic representation of the experimental procedure. (d) Mechanism of in situ encapsulation of PW in EG via microwave irradiation.

pores of the EG. The mixture of EG, the remaining un-expanded Eg, and PW were stirred evenly for around 20 s and irradiated for an additional 30 s. This irradiation-stir cycle was repeated until the full expansion of the Eg. The resulting EG-encapsulated PW mixture was then molded and pressed into specimens of varying shapes for characterization and applications. The duration required for the process can be significantly affected by factors such as the sample size and the power of the microwave irradiation. For instance, the creation of a 40 g PW/EG-10 % composite using 1100 W microwave irradiation necessitated an approximate total irradiation time of 10 min. In scenarios where scaling up is required, we could modify the microwave power to ensure that the duration of the irradiation process remains within a few minutes. This is considerably more time-efficient compared to the traditional impregnation method, which necessitates several hours of soaking time even for samples of a smaller scale.

2.3. Material structure characterization

The morphologies of Eg, EG, and PW/EG composites were analyzed using field-emission scanning electron microscopy (FE-SEM; JEOL JSM-7500F). A cross-section sample was prepared using freeze fracturing, where the samples were frozen in liquid nitrogen (−196 °C), followed by cracking. Samples were sputter-coated with 4 nm gold (Cressington 208HR) before imaging. The chemical structures of the composites were analyzed using Fourier transform infrared spectroscopy (FTIR; Bruker ALPHA-Platinum, Attenuated Total Reflection mode), with spectra recorded in the range of 4000–400 cm^{-1} at a resolution of 4 cm^{-1}. The crystalline structures of the composites were analyzed using X-ray diffraction (XRD; Rigaku MiniFlex, 3°–80°).

2.4. Thermal energy storage characterization

Leakage was assessed by maintaining samples at 80 °C and recording their mass at different time intervals. The form-stability of PCM composites was assessed by placing samples on a metal foil or mesh and monitoring shape changes at temperatures ranging from 30 to 80 °C. Thermographic images were obtained using an infrared thermal camera (FLIR A325sc). The thermal conductivity of PW/EG composites was measured using a Hot Disk Thermal Conductivity Analyzer (TPS 2500S; ThermTest Inc). Three repeated measurements have been conducted to calculate the average value and error bar. The thermal energy storage properties of the composites were analyzed using differential scanning calorimetry (DSC; TA Q20), with tests performed under a nitrogen atmosphere in the scanning range of 0–100 °C at a rate of 5 °C/min.

2.5. Demonstration of PW/EG composite-covered TE module

The PW/EG composite-covered TE module was fabricated by assembling a cuboid PW/EG composite (40 × 40 × 5 mm) on top of a thermoelectric (TE) module (TEC1-12706; 40 × 40 × 3.2 mm). A hot plate was used as a heat source. Temperature profiles at the hot and cold ends of TE modules were recorded using a thermocouple data logger (Sable Systems; TC-2000). The output voltages of the thermoelectric generator were recorded using a Keithley 2400 Instrument. The voltage and power of the TE modules were evaluated and compared with and without the presence of PW/EG composite.

3. Results and discussion

3.1. In situ encapsulation of PW within EG

This study presents a one-pot method for the in situ encapsulation of phase change materials (PCMs) to prevent leakage and enhance thermal conductivity (Fig. 2c). EG-encapsulated PW composites were prepared by filling EG pores with molten PW during the expansion of Eg. This was achieved by placing Eg in molten PW and subjecting it to microwave

irradiation. During irradiation, the electrically conductive graphene sheets within Eg generate strong eddy currents, leading to localized rapid heating [36]. When the local temperature exceeds 180 °C, intercalations between graphene layers gasify and generate gases (nitrogen oxides and sulfur oxides), separating the graphene layers and creating voids. As the expansion process occurs in molten PW, when gas escapes from the graphite interlayer, molten PW near the pores is drawn into the void left by the escaping gas due to the pressure difference (Fig. 2d), resulting in the in situ encapsulation of PW within EG pores.

The experimental process for fabricating PW/EG composites using the in situ encapsulation method is illustrated in Fig. 3a and Fig. S3. A beaker containing a mixture of 90 wt% molten PW and 10 wt% Eg was placed in a domestic microwave oven. After 30 s of microwave irradiation, some Eg expanded into EG and floated to the top of the molten PW, while most remained at the bottom of the beaker (Supplementary video 2). During the irradiation-expansion process, the vacuum void within the newly formed EG was filled with PW due to the pressure difference, forming an EG-encapsulated PW mixture (Fig. 3b). After stirring, the floating PW/EG mixture was mixed again with unexpanded Eg and unencapsulated molten PW (Fig. S4a). With increasing irradiation-stirring cycles (Fig. S4b–d), more PW/Eg became EG-encapsulated PW. After 7 min of intermittent irradiation-stirring treatment, almost all molten PW was encapsulated (Fig. S4e). Continuing with the irradiation-stirring process, additional layers of EG were wrapped around the EG-encapsulated PW, which is expected to further improve leakage resistance and thermal conductivity. After 10 min of intermittent irradiation-stirring treatment, all Eg had fully expanded. The resulting PW/EG mixture appeared as dry separated particles approximately 1 mm in size (Fig. 3c, and Fig. S4f). PW/EG composites of various shapes were prepared by compression molding (Fig. 3c-vi, and Fig. 3d). FT-IR and XRD results (figs. S5 and S6) showed that the chemical functional groups and crystal structure of PW remained unchanged before and after encapsulation, indicating that no chemical reaction occurred between PW and EG [13,44] and that the encapsulation method is a physical process.

3.2. *Influence of EG proportion on thermal energy storage characteristics of PW/EG composite*

Key performance indicators for phase change materials (PCMs) in thermal energy storage systems include shape stability, leakage resistance during thermal cycling, thermal conductivity, cycle durability, and latent heat storage capacity. For EG-encapsulated PCM composites, latent heat storage capacity is positively correlated with the proportion of PCM, while other performance indicators related to thermal stability depend on the proportion of EG. As such, there is a trade-off between latent heat storage capacity and thermal stability.

To investigate the effects of EG proportion on the thermal energy storage characteristics of PW/EG composites, PW/EG composites with varying EG mass fractions (0–20 wt%) were prepared and characterized

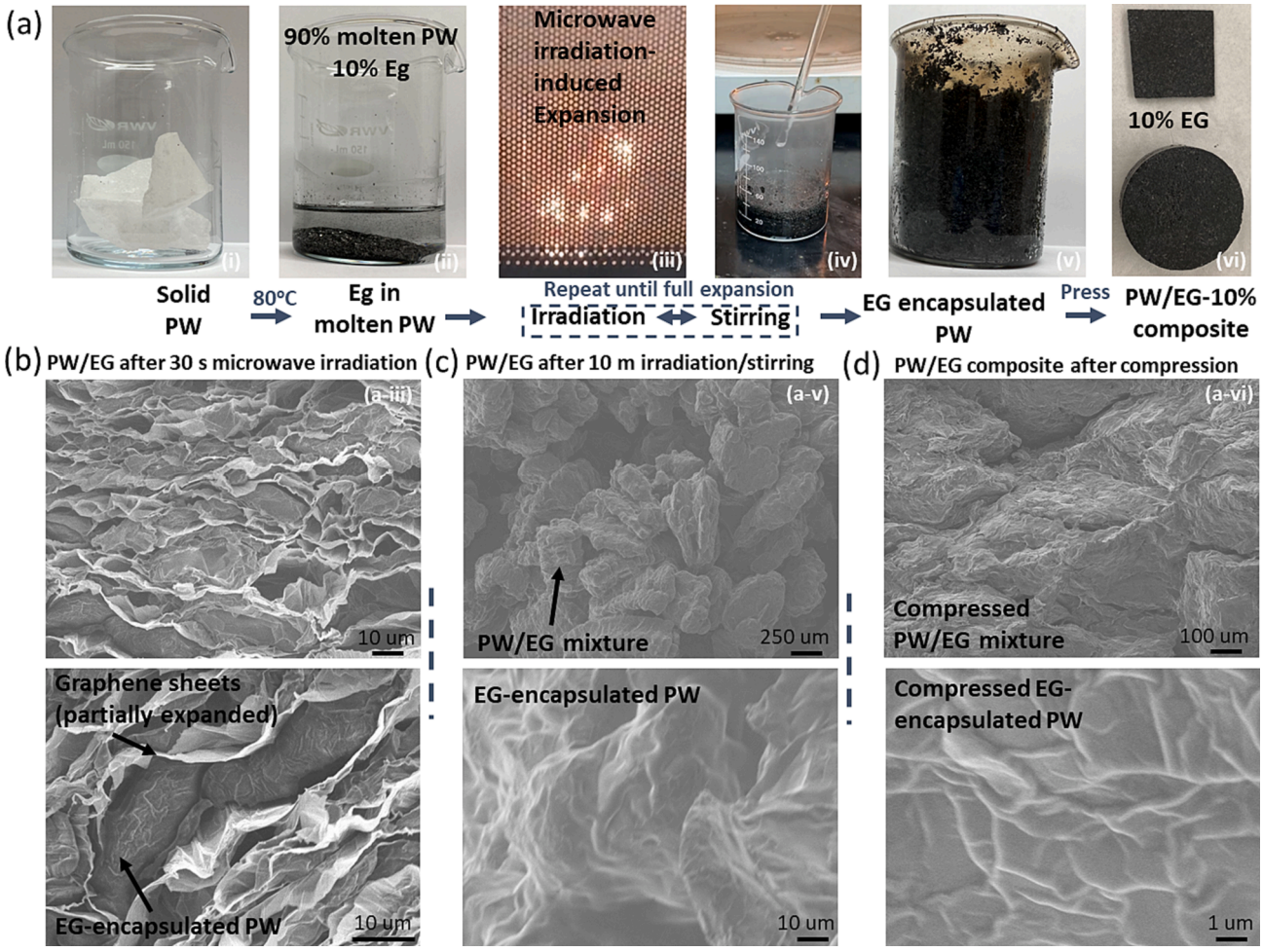

Fig. 3. In situ encapsulation of PW in EG (10 wt% content) via microwave irradiation. (a) Photographs of the experimental steps for the in situ encapsulation of PW with Eg by microwave irradiation. (b) SEM images of EG-encapsulated PW after 30 s microwave irradiation. (c) SEM image of the PW/EG mixture after intermittent microwave irradiation and stirring for 10 min. (d) SEM images of the PW/EG composite following the compression molding treatment, which exhibits reduced porosity.

(Table S2). The cross-sectional morphologies of PW/EG composites with different proportions of EG are shown in Fig. 3d and Fig. 4. When the EG proportion is 2 wt% and 5 wt%, the cross-sectional SEMs of the PW/EG composites show distinct strip-like and block-like PW clusters (Fig. 4a and b), due to the low proportion of EG being unable to absorb all the PW, resulting in some PW gathering on the surface of EG. As the EG proportion increases (8–10 wt%), the microporous structures of EG provide sufficient voids to contain the PW, ensuring good shape stability and leakage prevention performance. However, when the EG proportion is too high (15–20 wt%), unfilled voids remain (Fig. 4c and d), leading to high porosity in the PW/EG composites.

The densities and porosities of PW/EG composites with different EG mass fractions are shown in Fig. 4e and f. The porosity (P) of the composite was calculated using:

$$P = 1 - \frac{\rho}{\rho_t} \tag{1}$$

where ρ is the measured density of the composite, which was calculated by dividing the measured mass by the measured volume. ρ_t is the theoretical density assuming zero porosity, which was calculated using:

$$\rho_t = \eta_{EG}\rho_{EG} + (1 - \eta_{EG})\rho_{PW} \tag{2}$$

where η_{EG} is the mass fractions of EG in the binary PW/EG composites, which is determined by the feed mass ratio of Eg and solid PW. $\rho_{EG} = 2.26$ g/cm^3 and $\rho_{PW} = 0.852$ g/cm^3 are the densities of graphite and pure PW, respectively. As the mass fraction of EG increased from 2 wt% to 10 wt%, the porosity of the PW/EG composite increased from 8.45 % to 28.3 %, primarily due to the supersaturation of the pores of EG. When the mass fraction of EG reached 20 wt%, the porosity of the composite reached 49.7 %. The thermal energy storage characteristics of PW/EG composites would vary depending on their porosity.

Shape stability and leakage resistance during melting/freezing are essential for the practical application of TESS, particularly in scenarios where volume change is limited. To evaluate shape stability and leakage prevention performance during the solid–liquid phase transition, PW/EG composite samples with different EG mass fractions (0–20 wt%) were placed on aluminum foil or metal mesh and kept at 80 °C to ensure the solid–liquid phase transition (Fig. 5a and Fig. S7). After 1 min at 80 °C, pure PW had completely melted, while PW/EG composites containing 2 wt% and 5 wt% EG began to soften and deform. PW/EG composites with an EG content higher than 8 wt% maintained good shape stability without leakage. The mass retention ratio (r_m) of the PW/EG composites during leakage test was determined as follows:

$$r_m = \frac{m_t}{m_0} \tag{3}$$

where m_0 represents the initial mass of the PW/EG composites before placement on the hot plate (80 °C), and m_t denotes the mass of the PW/EG composites after being on the hot plate for specific durations. It was observed that the mass retention of PW/EG composites with an EG content exceeding 8 wt% remained above 99 %, even after 48 h at 80 °C (Fig. 5b). The minimum mass fraction of EG required to maintain shape

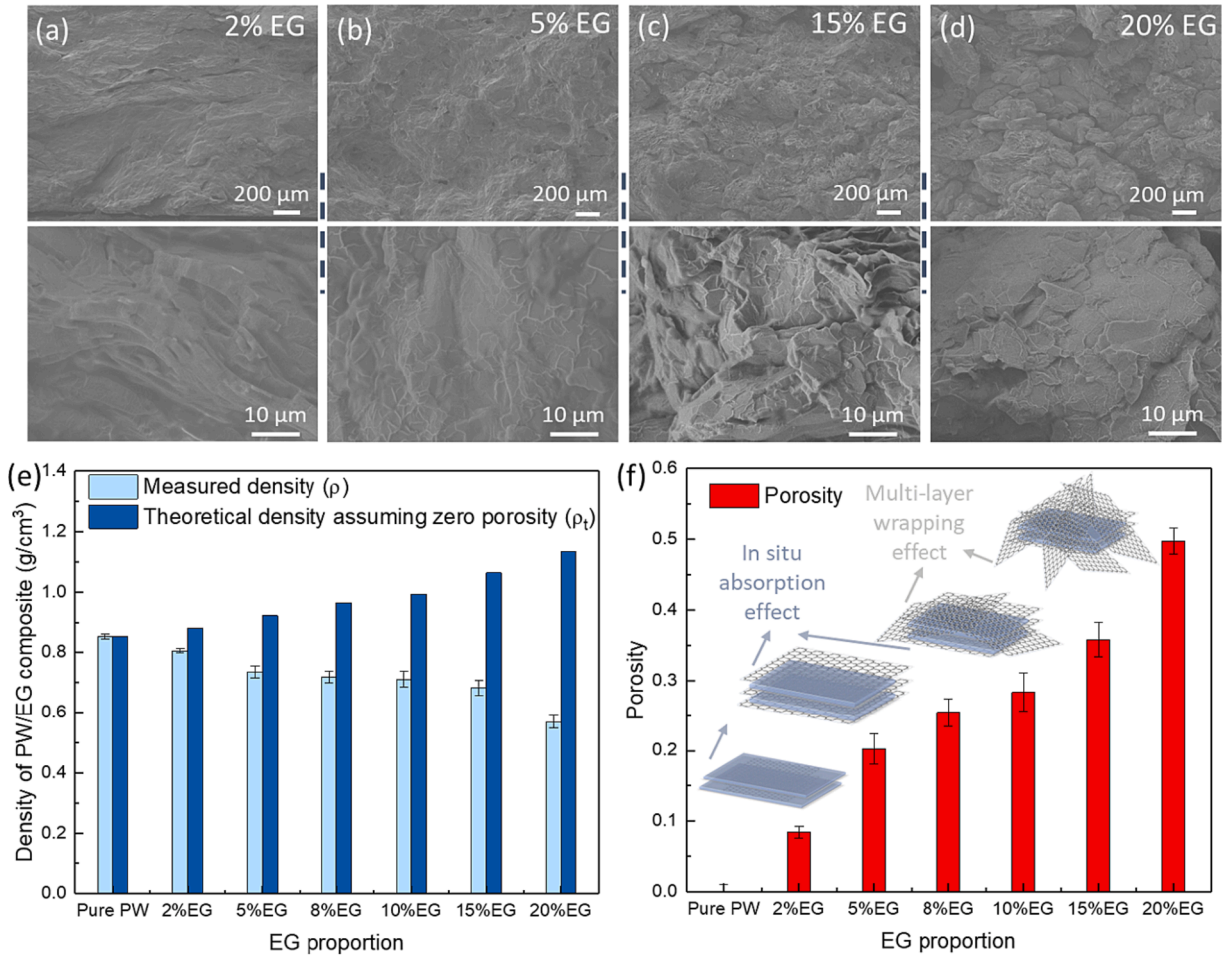

Fig. 4. Effects of EG proportion on the structure of PW/EG Composites. SEM images of PW/EG composites with (a) 2 wt% EG content, (b) 5 wt% EG content, (c) 15 wt% EG content, and (d) 20 wt% EG content. (e) Measured density and theoretical density of PW/EG composites with different EG proportions. (f) The porosity of PW/EG composites with different EG proportions. The inserted schematics illustrate the structures of PW/EG composites with different proportions of EG.

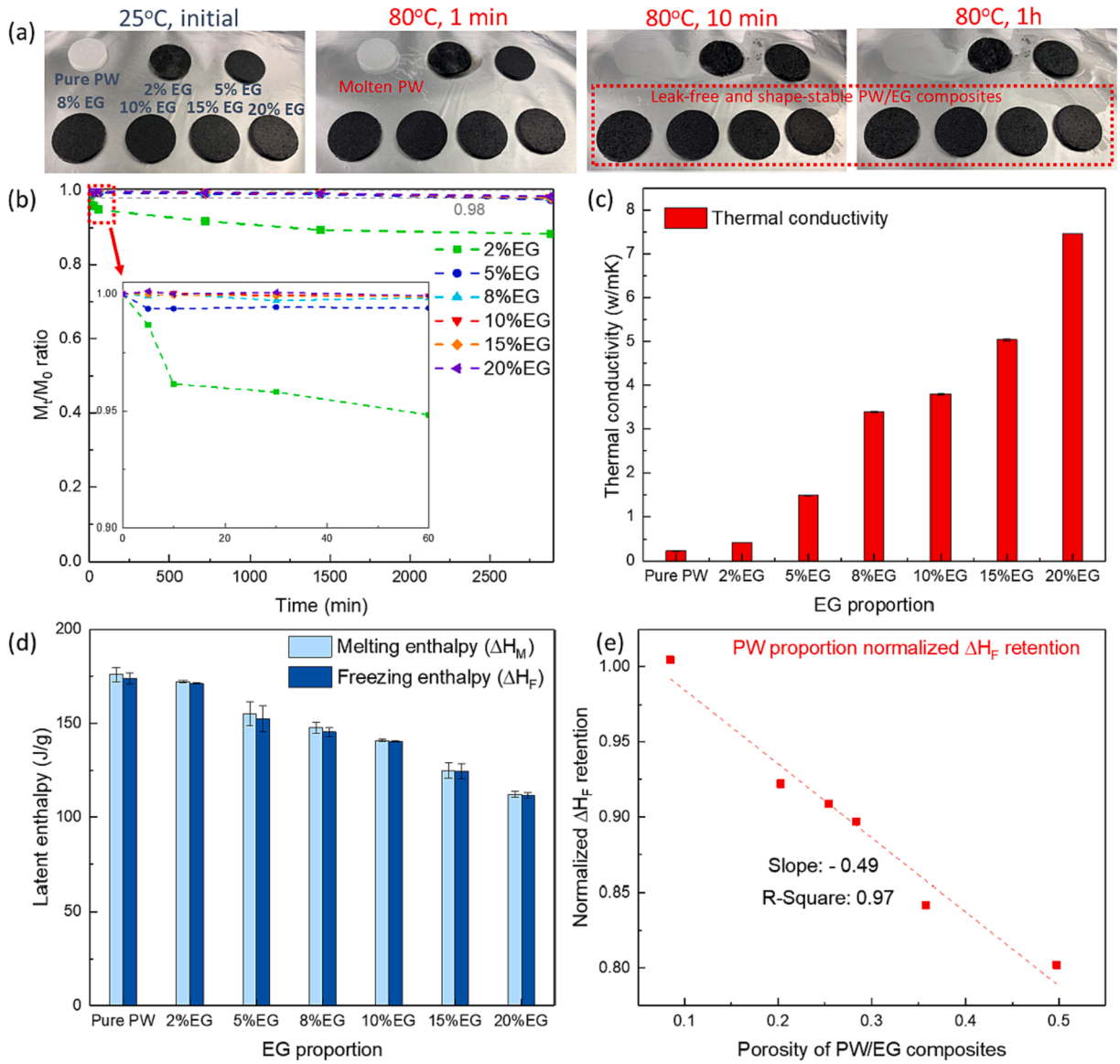

Fig. 5. Effect of EG proportion on Thermal Energy Storage Properties of PW/EG Composite. (a) Optical images of PW/EG composites heated on a hot plate maintained at 80 °C for varying durations. (b) Mass leakage over time, (c) Thermal conductivity, (d) Melting and freezing enthalpies of PW/EG composites with different EG proportions. (e) The linear fitting of porosity of PW/EG composite and normalized melting enthalpy retention.

stability in PW/EG composites prepared using the in situ encapsulation method in this study is 8 wt%, which is significantly lower than the approximately 20 wt% commonly reported for PW/EG composites [8] prepared using the impregnation method (Figs. S8 and S9). This can be primarily attributed to the high PCM absorption efficiency of EG during the in-situ encapsulation process, and the multilayer wrapping effect of excess EG during the intermittent irradiation-stirring process (Fig. 4f).

Thermal conductivity is a crucial parameter for assessing the thermal energy storage performance of TESS. Enhanced thermal conductivity facilitates more rapid and efficient heat transfer. However, the low thermal conductivity of pure PW, at just 0.233 W/mK, hinders its use in thermal energy storage. By incorporating EG, the thermal conductivity of PW can be significantly increased due to the formation of a continuous thermal bridge structure [45]. For EG mass fractions of 2, 5, 8, 10, 15, and 20 wt%, the thermal conductivities of PW/EG composites were found to be 0.43, 1.48, 3.39, 3.79, 5.03, and 7.46 W/mK, respectively (Fig. 5c). Compared to PW/EG composites prepared using the impregnation method (Fig. 1b), the composites prepared in this study using the in-situ encapsulation method demonstrated higher thermal conductivity for equivalent EG mass fractions. This is primarily due to the multilayer wrapping effect of excess EG during the intermittent irradiation-stirring process, which enhances the thermal bridge effect.

The energy storage properties of PW/EG composites, including melting enthalpy (ΔH_M), freezing enthalpy (ΔH_F), peak melting temperature (T_M), peak freezing temperature (T_F), and subcooling temperature (T_M-T_F), were evaluated using DSC (Fig. S10). Due to its higher thermal conductivity, the melting temperature of the PW/EG composite is lower than that of pure PW (Fig. S11), leading to a favorable reduction in the supercooling temperature [8]. As the EG mass fraction increases, the peak area of DSC decreases, indicating a decrease in the latent heat of phase transition for the PW/EG composite. The ratio of freezing enthalpy to melting enthalpy ($\Delta H_F/\Delta H_M$) exceeds 98 % for all PW/EG composites, indicating the high thermal release/absorption efficiency of PW/EG composites as thermal energy storage materials (Fig. 5d). The latent heat of the PW/EG composite is influenced by factors such as the latent heat of pure PW, the proportion of pure PW in the composite, and the composite's porosity. The freezing enthalpy for the PW/EG composite at 10 wt% EG is 140.37 J/g, which is 80.7 % of the 175.85 J/g for

pure PW and is lower than 90 wt% of the mass fraction of PW in the composite. When the EG mass fraction is increased to 20 wt%, the ratio of melting enthalpy (111.55 J/g) for the composite to that of pure PW drops to 64.2 %, significantly lower than 80 wt% of the mass fraction of PW.

To investigate the impact of porosity on the latent heat of the PW/EG composite, we established the ratio of the freezing enthalpy of the PW/EG composite to that of pure PW. This ratio is referred to as the ΔH_F retention of the PW/EG composite. We then compared this ratio to the corresponding ratio of PW proportions, a value we defined as normalized ΔHF retention. As shown in Fig. 5e, there is a linear and negative correlation between porosity and normalized ΔH_F retention for PW/EG composites, with a slope of −0.49 and an R-square value of 0.97 for its linear fit. The porosity of the PW/EG composite results in some PW covering the surface of graphene walls within EG, forming a thin coating. The molecular freedom of these PWs covered on the graphene surface is limited by the graphene surface, resulting in an incomplete solidified crystal structure and lower latent heat [46]. Increasing the amount of EG in the PW/EG composites leads to an increase in their porosity and specific surface area. This causes more PW to be constrained by the surface tension of graphene, resulting in lower normalized ΔH_F retention. A PW/EG composite with an EG content of 10 wt% can simultaneously achieve shape stability, high thermal conductivity, and good latent heat, making it suitable for further research.

3.3. Cyclic heating-cooling performance of PW/EG composites

PCMs for TESS must be able to withstand repeated heating and cooling cycles without degradation in thermal energy storage properties. The thermal cycling performance of pure PW and PW/EG composites was investigated using DSC through continuous heating and cooling cycle tests (Fig. 6 and Fig. S12). For pure PW, the DSC curves for the first thermal cycle differ significantly from those for subsequent cycles, primarily due to its poor shape stability. During the first heating, the melted PW spread inside the DSC crucible (the inserted image in Fig. 6a). In subsequent DSC tests, its shape remains relatively stable, resulting in high repeatability for its DSC curves. The melting and freezing enthalpy of pure PW remained relatively constant during 2 to 50 thermal cycles, indicating that pure PW can withstand repeated heating and cooling cycles without degradation in heat storage performance. PW/EG composites containing 10 wt% EG were prepared using in situ microwave irradiation (PW/EG-10 % composite), and their DSC curves showed little change during 100 thermal cycles, demonstrating excellent cyclic heat storage without degradation, excellent shape stability, and good leak resistance. After 100 cycles, both latent heat and phase transition temperature remained almost constant, indicating thermal stability over time, making the PW/EG-10 % composite an ideal thermal energy storage medium for practical scenarios. The excellent thermal cycling performance of the PW/EG-10 % composite is primarily due to its unique multilayer graphene-wrapped EG-encapsulated PW structure (Fig. 4f), which prevents leakage and performance degradation during cyclic thermal operation.

3.4. PW/EG-10 % composite covered TE modules for heat storage and recovery

A huge amount of waste heat is widely available from natural resources or industries [47,48]. Thermoelectric (TE) modules can be used to convert waste heat into electricity, thereby improving energy efficiency, reducing greenhouse gas emissions, and promoting decarbonization. According to the Seebeck effect, the output voltage of a TE module is positively related to the temperature gradient (ΔT) between its hot end and cold sink [49]. Under passive cooling, when a heat source is provided to the hot end of a TE module, its cold end temperature increases rapidly due to its high thermal conductivity, resulting in a low ΔT and low output voltage (Fig. 7a). Additionally, waste heat sources are often intermittent, leading to unstable output voltage and limiting the application of TE modules in waste heat recovery [50]. Therefore,

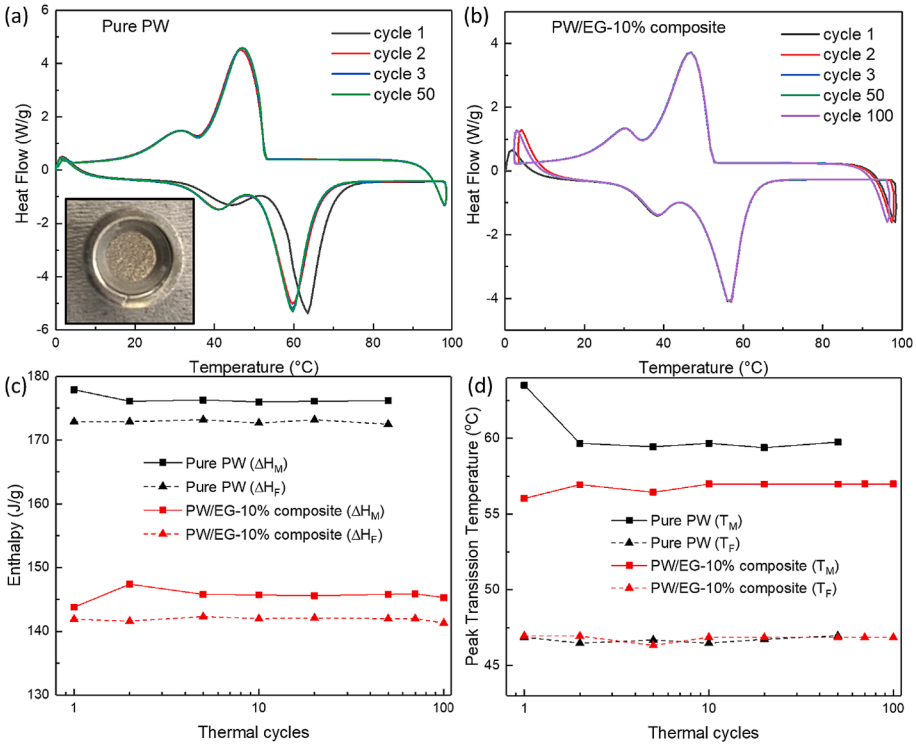

Fig. 6. Cyclic Heating-Cooling Performance of PW/EG-10% Composite. (a) DSC curves for 50 cyclic heating–cooling cycles of pure PW. (b) DSC curves for 100 cyclic heating–cooling cycles of PW/EG-10% composite prepared via the in situ microwave irradiation method. (c) Melting enthalpy (ΔH_M) and freezing enthalpy (ΔH_F), (d) Melting temperature (T_M) and freezing temperature (T_F) of pure PW and PW/EG-10% composite during thermal cycles.

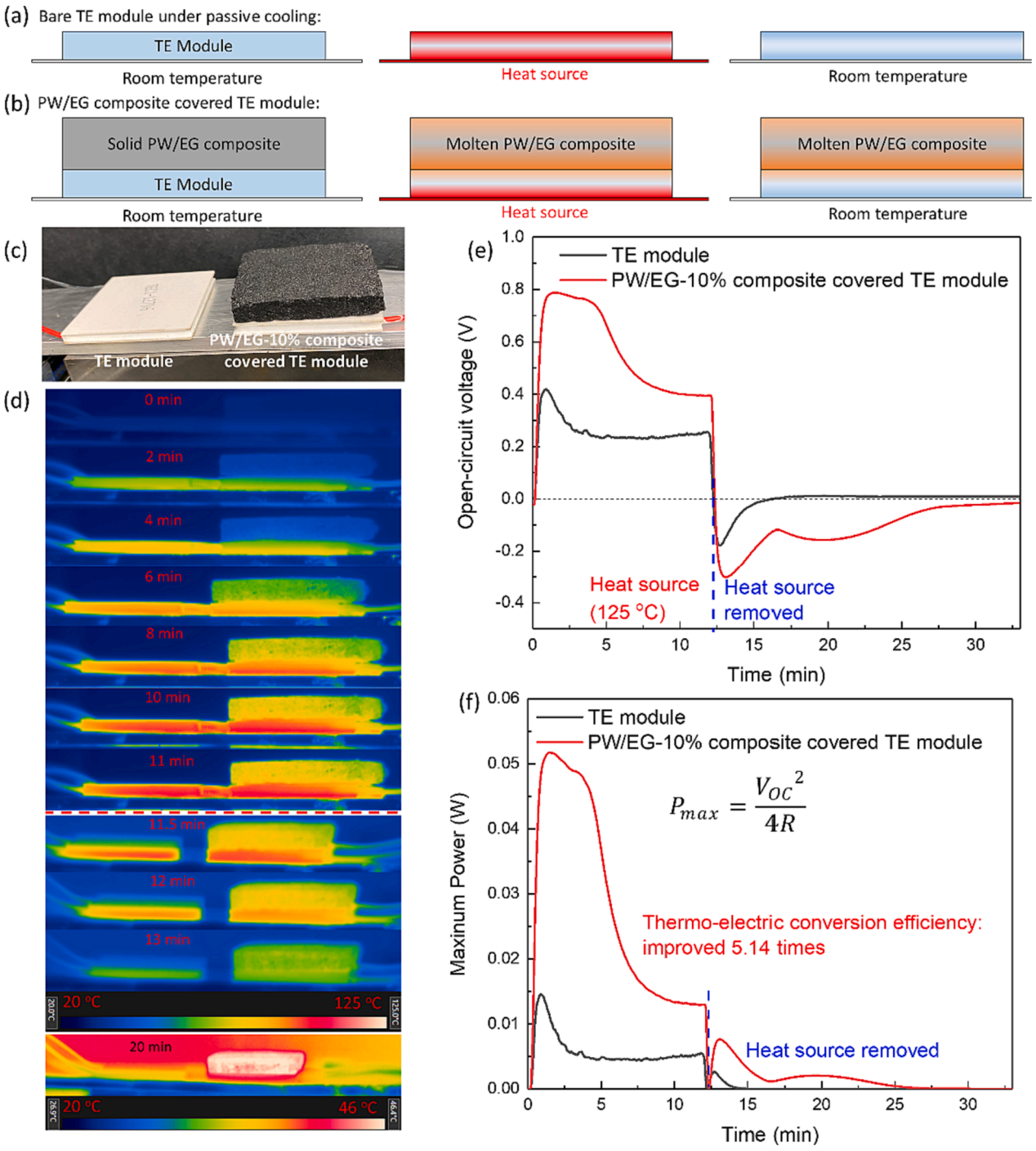

Fig. 7. PW/EG composite covered thermoelectric modules for heat storage and recovery. (a) Schematic diagram illustrating the temperature evolution of the TE module during the heat source on/off process. (b) Schematic diagram illustrating the temperature evolution of the PW/EG-TE module during the heat source on/off process. (c) Photographs of the bare TE module and the PW/EG-TE module. (d) Infrared images depicting the temperature evolution of both the bare TE module and the PW/EG-TE module during the heat source on/off process. (e) Output voltage, (f) Maximum output power and electricity generated by the bare TE module and the PW/EG-10 % composite covered TE module during the heat source on/off process. The heat source temperature was set at 125 °C.

there is an urgent need to develop a cost-effective method to maintain the ΔT of TE modules and overcome the intermittency of waste heat sources.

The PW/EG composite can be attached at the cold end of the TE module, which can serve as a TESS to maintain the temperature of the cold end of the TE module and mitigate the intermittency of the heat source (Fig. 7b). When a heat source is provided, the temperature at the cold sink of the TE module can be maintained at the melting temperature of the PCM. Compared to bare TE modules under passive cooling, a PW/EG composite-covered TE module (PW/EG-TE module) can generate a higher ΔT and larger output voltage. Moreover, when the heat source for the PW/EG-TE module is removed, the temperature at the former hot end drops to room temperature, while the former cold end remains at the melting temperature of PW, resulting in a reversed ΔT and output voltage. This PW/EG-TE module is expected to enhance thermoelectric conversion performance and serve as an energy storage system to mitigate the intermittency of waste heat in practical applications.

To test the concept, a PW/EG composite was assembled on a

commercial TE module, as shown in Fig. 7c and Fig. S13. A second bare TE module with identical technical specifications was used as a control and subjected to the same heat source. Upon placing on a hot plate (125 °C), the temperatures at both the hot (bottom side) and cold (top side) ends of the bare TE module increased rapidly, resulting in a ΔT of approximately 20 °C. However, this ΔT decreased to approximately 10 °C within 2 min. When subjected to the heat source, the output voltage of the TE module rapidly increased to 0.4 V within 30 s before decreasing to 0.22 V within 2 min. Upon removal of the heat source and stabilization of the temperature at room temperature, the bare TE module generated a reverse voltage of approximately −0.2 V, which subsequently decreased to 0 within 2 min, as shown in Fig. 7d and e. In contrast, when subjected to the same heat source, the PW/EG-TE module reached a peak ΔT of approximately 40 °C, generating an output voltage of approximately 0.85 V. After 10 min, the temperature of the upper side stabilized at approximately 60 °C, which corresponds to the melting temperature of the PW, resulting in an ΔT of approximately 20 °C and an output voltage of approximately 0.45 V. Upon removal of the heat source and stabilization of the temperature at room temperature, the PW/EG-TE module generated a reverse voltage of approximately −0.3 V, which gradually decreased to approximately −0.03 V within 20 min.

The power of the bare TE module and PW/EG-TE module during the heat source on–off process was calculated using:

$$P_{max} = \frac{{V_{OC}}^2}{4R} \tag{4}$$

where R = 3 Ω is the internal resistance of the TE module, as illustrated in Fig. 7f. The electricity generated during the heat source on–off process was calculated by integrating the power-time curve. During the heat source on–off process, the electricity generated by the bare TE module was 0.073 J. In contrast, the electricity generated by the PW/EG-TE module was 0.375 J, which is 5.14 times higher than that generated by the bare TE module under the same heat source on–off process. These results demonstrate that PW/EG composite can effectively enhance the thermo-electric conversion performance of the TE module and expand their practical applications.

4. Conclusion

This study has effectively demonstrated a rapid and energy-efficient one-pot encapsulation method for the in situ encapsulation of paraffin wax (PW) within the pores of expanded graphite (EG) using microwave irradiation. This innovative approach addresses the challenges associated with traditional impregnation-based encapsulation processes, which are both time-consuming and energy-intensive. The PW/EG composites produced through this method exhibit impressive shape stability, no leakage even at high PW loading, and significantly enhanced thermal conductivity. Specifically, the PW/EG composite with 10 wt% EG showcases a thermal conductivity of 3.7 W/mK, which is 16.2 times higher than that of pure PW, a thermal release/absorption efficiency of approximately 99.5 %, and nearly 100 % capacity retention after thermal cycling. Furthermore, integrating PW/EG TESS with thermoelectric (TE) modules has been shown to increase TE power generation by five-fold, highlighting the potential of these composites in energy storage and conversion applications. This one-pot encapsulation method holds promise as a foundational technology for encapsulating various energy storage materials such as salt hydrates and fatty acids, thereby promoting decarbonization. Consequently, this work paves the way towards mitigating the intermittency of renewable energy generation and achieving net-zero greenhouse gas emissions.

CRediT authorship contribution statement

Wei Li: Conceptualization, Methodology, Investigation, Data curation, Formal analysis, Validation, Writing – original draft, Writing – review & editing. **Chongjie Gao:** Investigation. **Aolin Hou:** Investigation. **Jingjing Qiu:** Methodology, Resources, Writing – review & editing. **Shiren Wang:** Conceptualization, Funding acquisition, Methodology, Supervision, Writing – review & editing.

Declaration of competing interest

The authors declare that they have no known competing financial interests or personal relationships that could have appeared to influence the work reported in this paper.

Data availability

Data will be made available on request.

Acknowledgment

This work is partially supported by the National Science Foundation (CMMI-1934120, CMMI-1933679).

Appendix A. Supplementary data

Supplementary data to this article can be found online at https://doi.org/10.1016/j.cej.2024.148541.

References

[1] W. Fu, X. Yan, Y. Gurumukhi, V.S. Garimella, W.P. King, N. Miljkovic, High power and energy density dynamic phase change materials using pressure-enhanced close contact melting, Nat. Energy 7 (3) (2022) 270–280.
[2] F. Grassauer, V. Arulnathan, N. Pelletier, Towards a net-zero greenhouse gas emission egg industry: a review of relevant mitigation technologies and strategies, current emission reduction potential, and future research needs, Renew. Sustain. Energy Rev. 181 (2023) 113322.
[3] W. Li, J. Ma, J. Qiu, S. Wang, Thermocells-enabled low-grade heat harvesting: challenge, progress, and prospects, Mater. Today Energy 27 (2022) 101032.
[4] J. Li, M.S. Ho, C. Xie, N. Stern, China's flexibility challenge in achieving carbon neutrality by 2060, Renew. Sustain. Energy Rev. 158 (2022) 112112.
[5] A. Martin, D. Lilley, R. Prasher, S. Kaur, Particle size optimization of thermochemical salt hydrates for high energy density thermal storage, Energy Environ. Mater. e12544.
[6] C. Liu, Y. Song, Z. Xu, J. Zhao, Z. Rao, Highly efficient thermal energy storage enabled by a hierarchical structured hypercrosslinked polymer/expanded graphite composite, Int. J. Heat Mass Transfer 148 (2020) 119068.
[7] Q. Wang, D. Zhou, Y. Chen, P. Eames, Z. Wu, Characterization and effects of thermal cycling on the properties of paraffin/expanded graphite composites, Renew. Energy 147 (2020) 1131–1138.
[8] Y. Zhao, L. Jin, B. Zou, G. Qiao, T. Zhang, L. Cong, F. Jiang, C. Li, Y. Huang, Y. Ding, Expanded graphite–Paraffin composite phase change materials: effect of particle size on the composite structure and properties, Appl. Therm. Eng. 171 (2020) 115015.
[9] G. Fang, M. Yu, K. Meng, F. Shang, X. Tan, High-performance phase-change materials based on paraffin and expanded graphite for solar thermal energy storage, Energy Fuel 34 (8) (2020) 10109–10119.
[10] X. Tang, J. Zhang, J. Wang, T. Xu, Y. Du, G. Fan, H. Wu, Preparation and application of paraffin/expanded graphite-based phase change material floor for solar-heat pump combined radiant heating systems, ACS Sustain. Chem. Eng. (2023).
[11] S. Tian, S. Wu, S. Cui, Y. Tian, K.J. Balkus, L. Zhou, G. Xiong, High-performance solid-state supercapacitors integrated with thermal management systems based on phase change materials: all in one, Chem. Eng. J. 446 (2022) 136787.
[12] X. Cao, C. Li, Y. Li, Y. Tong, G. He, Z. Yang, Novel paraffin wax/ultra-high molecular weight polyethylene composite phase change materials modified by carbon nanotubes with excellent combination property, J. Appl. Polym. Sci. 139 (5) (2022) 51564.
[13] Y. Xie, Y. Yang, Y. Liu, S. Wang, X. Guo, H. Wang, D. Cao, Paraffin/polyethylene/graphite composite phase change materials with enhanced thermal conductivity and leakage-proof, Adv. Compos. Hybrid Mater. 4 (2021) 543–551.
[14] F. Cheng, Y. Xu, Z. Lv, Z. Huang, M. Fang, Y.g. Liu, X. Wu, X. Min, Form-stable and tough paraffin-Al2O3/high density polyethylene composites as environment-friendly thermal energy storage materials: preparation, characterization and analysis, J. Therm. Anal. Calorim. 146 (2021) 2089–2099.
[15] H. Li, R.Y. Tay, S.H. Tsang, R. Hubert, P. Coquet, T. Merlet, J. Foncin, J.J. Yu, E.H. T. Teo, Thermally conductive and leakage-proof phase-change materials composed of dense graphene foam and paraffin for thermal management, ACS Appl. Nano Mater. 5 (6) (2022) 8362–8370.

[16] D. Zhou, S. Xiao, X. Xiao, Preparation and thermal performance of fatty acid binary eutectic mixture/expanded graphite composites as form-stable phase change materials for thermal energy storage, ACS Omega (2023).
[17] T. Xiao, Q. Liu, Y. Lin, T. Lin, J. Zhao, W. Sun, X. Chen, C. Liu, In situ encapsulation of phase-change thermal-storage material using 3D polymer-aided cross-linked porous carbon, Adv. Energy Sustain. Res. (2022) 2200164.
[18] X. Liu, H. Su, Z. Huang, P. Lin, T. Yin, X. Sheng, Y. Chen, Biomass-based phase change material gels demonstrating solar-thermal conversion and thermal energy storage for thermoelectric power generation and personal thermal management, Sol. Energy 239 (2022) 307–318.
[19] Z. Niu, W. Yuan, Highly efficient thermo-and sunlight-driven energy storage for thermo-electric energy harvesting using sustainable nanocellulose-derived carbon aerogels embedded phase change materials, ACS Sustain. Chem. Eng. 7 (20) (2019) 17523–17534.
[20] L. Zhong, X. Zhang, Y. Luan, G. Wang, Y. Feng, D. Feng, Preparation and thermal properties of porous heterogeneous composite phase change materials based on molten salts/expanded graphite, Sol. Energy 107 (2014) 63–73.
[21] T. Zou, X. Liang, S. Wang, X. Gao, Z. Zhang, Y. Fang, Effect of expanded graphite size on performances of modified CaCl2· 6H2O phase change material for cold energy storage, Microporous Mesoporous Mater. 305 (2020) 110403.
[22] S. Wu, T. Yan, Z. Kuai, W. Pan, Experimental and numerical study of modified expanded graphite/hydrated salt phase change material for solar energy storage, Sol. Energy 205 (2020) 474–486.
[23] Y. Wu, T. Wang, Hydrated salts/expanded graphite composite with high thermal conductivity as a shape-stabilized phase change material for thermal energy storage, Energ. Conver. Manage. 101 (2015) 164–171.
[24] X. Qi, T. Zhu, W. Hu, W. Jiang, J. Yang, Q. Lin, Y. Wang, Multifunctional polyacrylamide/hydrated salt/MXene phase change hydrogels with high thermal energy storage, photothermal conversion capability and strain sensitivity for personal healthcare, Compos. Sci. Technol. 234 (2023) 109947.
[25] Y. Li, C. Li, N. Lin, B. Xie, D. Zhang, J. Chen, Review on tailored phase change behavior of hydrated salt as phase change materials for energy storage, Mater. Today Energy 22 (2021) 100866.
[26] E. Barbosa, A.K. Menon, Thermodynamic and kinetic characterization of salt hydrates for thermochemical energy storage, MRS Commun. 12 (5) (2022) 678–685.
[27] A.A. ElBahloul, E.-S.-B. Zeidan, I.I. El-Sharkawy, A.M. Hamed, A. Radwan, Recent advances in multistage sorption thermal energy storage systems, J. Storage Mater. 45 (2022) 103683.
[28] S. Cui, R.A. Kishore, P. Kolari, Q. Zheng, S. Kaur, J. Vidal, R. Jackson, Model-driven development of durable and scalable thermal energy storage materials for buildings, Energy 265 (2023) 126339.
[29] D.G. Atinafu, Y.S. Ok, H.W. Kua, S. Kim, Thermal properties of composite organic phase change materials (PCMs): a critical review on their engineering chemistry, Appl. Therm. Eng. 181 (2020) 115960.
[30] Z. Yu, D. Feng, Y. Feng, X. Zhang, Thermal conductivity and energy storage capacity enhancement and bottleneck of shape-stabilized phase change composites with graphene foam and carbon nanotubes, Compos. A Appl. Sci. Manuf. 152 (2022) 106703.
[31] W. Wang, X. Yang, Y. Fang, J. Ding, J. Yan, Preparation and thermal properties of polyethylene glycol/expanded graphite blends for energy storage, Appl. Energy 86 (9) (2009) 1479–1483.
[32] W. Wu, W. Wu, S. Wang, Form-stable and thermally induced flexible composite phase change material for thermal energy storage and thermal management applications, Appl. Energy 236 (2019) 10–21.
[33] B.G. Van Ravensteijn, P.A. Donkers, R.C. Ruliaman, J. Eversdijk, H.R. Fischer, H. P. Huinink, O.C. Adan, Encapsulation of salt hydrates by polymer coatings for low-temperature heat storage applications, ACS Appl. Polym. Mater. 3 (4) (2021) 1712–1726.
[34] A. Shkatulov, R. Joosten, H. Fischer, H. Huinink, Core–shell encapsulation of salt hydrates into mesoporous silica shells for thermochemical energy storage, ACS Appl. Energy Mater. 3 (7) (2020) 6860–6869.
[35] A. Palacios, M.E. Navarro, C. Barreneche, Y. Ding, Water sorption-based thermochemical storage materials: a review from material candidates to manufacturing routes, Front. Therm. Eng. 2 (2022) 1003863.
[36] S. Tao, S. Wei, Y. Yulan, Characterization of expanded graphite microstructure and fabrication of composite phase-change material for energy storage, J. Mater. Civ. Eng. 27 (4) (2015) 04014156.
[37] Z. Zhang, N. Zhang, J. Peng, X. Fang, X. Gao, Y. Fang, Preparation and thermal energy storage properties of paraffin/expanded graphite composite phase change material, Appl. Energy 91 (1) (2012) 426–431.
[38] N. Verma, R. Kumar, S. Zafar, H. Pathak, Vacuum-assisted microwave curing of epoxy/carbon fiber composite: an attempt for defect reduction in processing, Manufacturing Lett. 24 (2020) 127–131.
[39] C. Li, B. Xie, J. Chen, Z. Chen, X. Sun, S.W. Gibb, H 2 O 2-microwave treated graphite stabilized stearic acid as a composite phase change material for thermal energy storage, RSC Adv. 7 (83) (2017) 52486–52495.
[40] I.E. Rivero, V. Balsamo, A.J. Müller, Microwave-assisted modification of starch for compatibilizing LLDPE/starch blends, Carbohydr. Polym. 75 (2) (2009) 343–350.
[41] S. Sundararajan, A.B. Samui, P.S. Kulkarni, Shape-stabilized poly (ethylene glycol) (PEG)-cellulose acetate blend preparation with superior PEG loading via microwave-assisted blending, Sol. Energy 144 (2017) 32–39.
[42] Z. Li, E. Gariboldi, Review on the temperature-dependent thermophysical properties of liquid paraffins and composite phase change materials with metallic porous structures, Mater. Today Energy 20 (2021) 100642.
[43] T. Jiang, Y. Zhang, S. Olayiwola, C. Lau, M. Fan, K. Ng, G. Tan, Biomass-derived porous carbons support in phase change materials for building energy efficiency: a review, Mater. Today Energy 23 (2022) 100905.
[44] Y. Zhang, W. Li, J. Huang, M. Cao, G. Du, Expanded graphite/paraffin/silicone rubber as high temperature form-stabilized phase change materials for thermal energy storage and thermal interface materials, Materials 13 (4) (2020) 894.
[45] X. Liu, Z. Rao, Experimental study on the thermal performance of graphene and exfoliated graphite sheet for thermal energy storage phase change material, Thermochim. Acta 647 (2017) 15–21.
[46] M.M. Umair, Y. Zhang, K. Iqbal, S. Zhang, B. Tang, Novel strategies and supporting materials applied to shape-stabilize organic phase change materials for thermal energy storage – a review, Appl. Energy 235 (2019) 846–873.
[47] W. Li, Y. Liu, Z. Zhang, R. Liu, J. Qiu, S. Wang, Thermo-osmotic ionogel enabled high-efficiency harvesting of low-grade heat, J. Mater. Chem. A 9 (28) (2021) 15755–15765.
[48] J. Duan, B. Yu, L. Huang, B. Hu, M. Xu, G. Feng, J. Zhou, Liquid-state thermocells: opportunities and challenges for low-grade heat harvesting, Joule 5 (4) (2021) 768–779.
[49] L. Wang, Z. Zhang, L. Geng, T. Yuan, Y. Liu, J. Guo, L. Fang, J. Qiu, S. Wang, Solution-printable fullerene/TiS 2 organic/inorganic hybrids for high-performance flexible n-type thermoelectrics, Energ. Environ. Sci. 11 (5) (2018) 1307–1317.
[50] W. Li, C. Gao, J. Ma, J. Qiu, S. Wang, Simultaneous enhancement of thermopower and ionic conductivity for N-type Fe (III/II) thermocell, Mater. Today Energy 30 (2022) 101147.